https://doi.org/10.5194/egusphere-2026-3450
Preprint. Discussion started: 7 August 2026

Optical 3D micro-scanning for the determination of the envelope volume of rock samples

Lena-Maria Able[1], Eric Salomon[2], Florian Duschl[1], Harald Stollhofen[2], Michael C. Drews[1]

[1]Professorship of Geothermal Technologies, Technical University of Munich, Munich, 80333, Germany
[2]GeoZentrum Nordbayern, Friedrich-Alexander-Universität Erlangen-Nürnberg, Erlangen, 91054, Germany

Correspondence to: Lena-Maria Able (lenamaria.able@tum.de)

Abstract The envelope volume of rock samples is a key parameter in petrophysical rock evaluation, e.g. to determine standard properties such as density and porosity. For irregularly shaped rock samples the envelope volume is typically determined by immersion weighing or, for soluble or swellable rock samples (i.e. evaporites or clay), by measuring the displacement of fluid-like granular particles, using an envelope density analyzer. In this study, we investigate the use of an optical 3D micro-scanner as a non-destructive method to determine the envelope volume of a variety of rock samples of sedimentary, igneous and metamorphic origin. An optical 3D micro-scanner records a point cloud of the rock sample's surface and uses the triangulation principle to recreate the surface – and thus volume – in a three-dimensional coordinate system. The optical 3D micro-scanner was evaluated regarding its suitability and reproducibility for imaging various surface properties and compared against envelope volume measurements using an envelope density analyzer. The results show that optical 3D micro-scanning performs best for samples with a low surface roughness, regardless of the color and brightness, while recessed angles or shiny surfaces increase inaccuracy. Nevertheless, the optical 3D micro-scanner always yields a higher reproducibility than the standard envelope density analyzer. We conclude that using optical 3D micro-scanning is a fast, non-destructive and reliable alternative for measuring the envelope volume of most rock samples.

1 Introduction

Petrophysical characterization of rock samples is of central importance in geosciences. Density and porosity are crucial petrophysical characteristics to assess the hydraulic and mechanical constitution and behavior of rocks (Jaeger et al., 2007; Zoback, 2007) and to even infer their geologic history (Allen and Allen, 2013; Sclatter and Christie, 1980; Bjørlykke, 2015).

Measuring density and porosity of rock sample always requires the determination of the specimen's envelope volume. In case the sample is cut into a precise Euclidean geometry (e.g. cuboid or cylinder), the envelope volume can be rather easily measured and calculated. However, many situations, such as small amounts of

https://doi.org/10.5194/egusphere-2026-3450
Preprint. Discussion started: 7 August 2026

available rock material (e.g. drill core fragments or cuttings), weakly consolidated sediments (e.g. sands, clays), extremely porous rocks (e.g. pumice), or highly irregular sample surfaces (e.g. breccia, scoria) do not allow such geometric sample preparation. In this case, the envelope volume is typically determined by measuring the displacement of a fluid or fluid-like material by the rock sample. But some of the commonly used methods may inherit disadvantages. For example, immersion weighing (Deutsches Institut für Normung, 2007) is frequently used, but involves a long preparation time, can alter properties of the sample in contact with water and thus cannot be used for rock samples which contain swellable or soluble minerals. Also, mercury porosimetry (Deutsches Institut für Normung, 2019) contaminates the sample with a hazardous substance, which creates high costs and prevents further use of the sample material. The standard non-destructive, non-alternating procedure to determine the envelope volume is achieved through analyzing the envelope density. Typical envelope density analyzers measure the difference in displacement of a plunger, which moves into a sample chamber of known volume and filled with a normed dry fluid-like medium. The measurement is carried out both, with and without the the rock sample (Micromeritics Instrument Corporation, 2017; Anton Paar GmbH).

Alternatively, the envelope volume can also be directly measured by collecting a 3D representation of the sample. The 3D micro-scanning method, which captures rather complex objects by emitting a specific light pattern by a projector and detection by a camera, was already established since the 1970s to measure the envelope volume of objects (e.g. Shirai, 1972; Agin, 1972; Agin and Highnam, 1983). Optical 3D-micro scanning can achieve high accuracy and reproducibility (Mendricky and Sobotka, 2020; Eiríksson et al., 2016). Today it is commonly used in product development as a part of reverse engineering (Várady et al., 1997; Sokovic and Kopac, 2006) or more recently in medical applications (Shamata and Thompson, 2018; Sivanandan and Liscio, 2016; Limones et al., 2025) or archeology (Diara, 2023; Gölder et al., 2022; Homburg et al., 2022). A new application is also the measurement of surface properties of rocks (Dietmaier et al., 2025), but the method has not been explicitly used for measuring the envelope volume of rock samples to determine their density and porosity, yet.

In this study, we test the suitability and reproducibility of optical 3D micro-scanning to determine the envelope volume of thirteen different rock samples which cover a wide range of textures, fabrics and geologic origin (sedimentary, igneous, metamorphic). The measurement procedure and results are compared to a standard envelope density analyzer and recommendations for measuring the envelope volume of the covered rock types are provided.

2 Methods

Our workflow to assess the suitability of an optical 3D micro-scanner to determine the envelope volume of rock samples is shown in Fig. 1. After preparation and weighing, the rock samples were measured three times with

https://doi.org/10.5194/egusphere-2026-3450
Preprint. Discussion started: 7 August 2026

both, the 3D micro-scanner and the envelope density analyzer, whereby the device settings were kept constant. This refers to the scan path and the type of fusion of the 3D micro-scanner as well as to the sample-to-medium ratio and the plunger force of the envelope density analyzer. Hereby, we also tested different measurement options (modified setup) to assess their impact on the reproducibility. In the following, the individual workflow steps are described in detail.

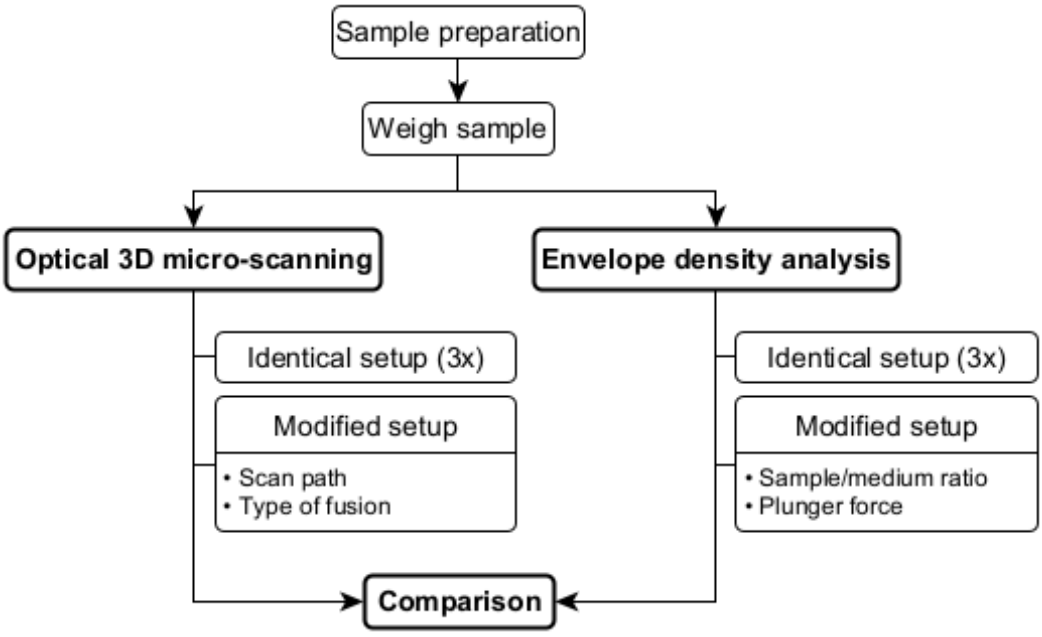

Figure 1: Workflow to test the ability of an optical 3D micro-scanner to measure the envelope volume of rock samples in comparison to the measurement using an envelope density analyzer, and in relation to porosity calculation.

2.1 Sample preparation and weighing

During formatting utmost care was exercised to ensure that samples a) fit equally into both devices resulting in dimensions which do not exceed 58 x 60 x 80 mm and b) preserve their characteristic natural surface attributes (e.g. high surface roughness, crystal planes, pore structures). To prevent swelling or dissolution due to contact with water during sawing, the samples were fragmented using a hammer if needed or sewn to generate a cubic geometry. The samples were then dried at 50 °C for 72 h to reduce the moisture content.

2.2 Optical 3D micro-scanning

The optical 3D micro-scanner used is the fully automatic, portable Artec Micro I (Artec 3D; Software Artec Studio 16 Professional, Version 16.0.8.2) with a pinpoint accuracy of ≥0.01 mm and a resolution of 0.029 mm (Artec 3D, 2020). Further specifications are listed in Appendix A.

https://doi.org/10.5194/egusphere-2026-3450
Preprint. Discussion started: 7 August 2026

Optical 3D micro-scanners use structured light to produce a digital three-dimensional point cloud of the scanned object, which then allows to determine the envelope volume of the object. To do so, a projector is emitting light by a LED source in a geometric pattern, in this case a high-contrast stripe pattern. When the light is projected onto the scanned object the geometric pattern is deformed, which in turn is captured by a camera. If positions of the camera and the projector are known, the position of every point on the sample can be determined based on the active triangulation principle (Fig. 2). Hereby, a specific point *P* is determined by the crossing of a coded stripe *ζ* (red stripe in Fig.2) projected onto the sample by the mirror *M* and a line with a specific coordinate orientation *u, v* starting from the camera *C* (Agin and Highnam, 1983; Chen and Kak, 1987; Rocchini et al., 2001; Wiora, 2001).

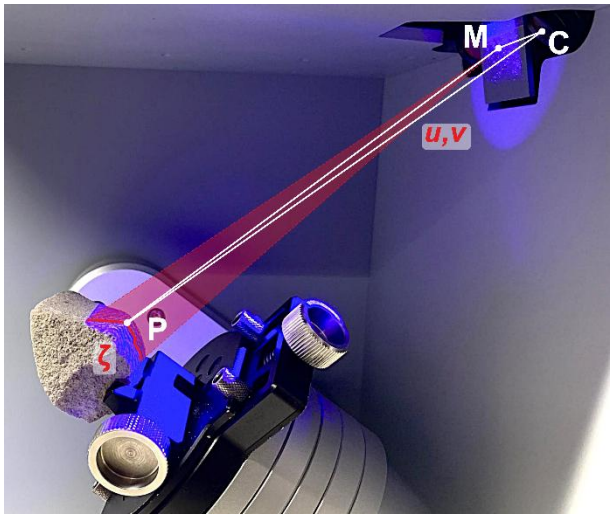

Figure 2: Triangulation principle of the 3D micro-scanner between the camera C, the mirror M and a point P of the rock sample. The mirror is reflecting the geometric pattern (red shade), emitted by the projector, onto the sample. The geometric stripe pattern is covering the area, which is visible for the scanning unit (Drawn after Chen and Kak, 1987; Georgopoulos et al., 2010; Wiora, 2001).

The scanned object, in this case a rock sample, must be attached between the jaws of the included vise or between the screws of the screw jig at the L-shaped arm. The maximal object size is limited to approximately 90 x 60 x 90 mm. After adjusting the brightness, the sample will be automatically scanned under various angels, during rotation around the two axes of the L-shaped arm. To ensure the best results possible, the scan path “small complex” (49 frames) was chosen, which is, according to the manufacturer (Artec 3D, 2019) the best fit for “object[s] no bigger than 5 cm with many difficult-to-reach areas and numerous geometrical irregularities”.

After the first scan, the sample is rotated in the vise so that the part where it was attached to the rotational system is captured in a second scan. The raw data must be edited to obtain the finished model, which involves the following procedures. First, the individual scans are manually cleared from unwanted artifacts. Then the scans must be aligned, so that they both have the same position and orientation. Afterwards the processed imagery is registered in a coordinate system. The aligned scans are merged to one model by using the “Fast

https://doi.org/10.5194/egusphere-2026-3450
Preprint. Discussion started: 7 August 2026

fusion" option (Artec 3D, 2019). If areas remain that could not be captured, additional scans can be added also after editing. Small, remaining holes in the generated scanned surface (referred to as "holes" in the following) are filled to create a closed surface for the measurement of the volume, which is realized by an automatic meshing process. Holes can either be filled all together or individually. Following this procedure, the surface area [mm^2] and the envelope volume [mm^3] of the sample are calculated automatically.

To test the reproducibility of the device we carried out three measurements for each sample and compared the results to the volumes determined with the envelope density analyzer. The scan path and the type of fusion were selected consistently for each rock sample.

The results of the chosen settings were also compared to the results of less and more precise ones to observe quantitative changes relative to each other. To do so, the scan path was changed to create less or more scans during measurements, and the type of fusion (i.e. "sharp fusion" instead of "fast fusion") was changed to check a potentially higher level of detail (cf. modified setup in Fig. 1).

2.3 Envelope density analysis

The optical 3D scanning method is compared to the envelope density analyzer GeoPyc 1365 (Micromeritics). The specifications of the latter are listed in Appendix B.

This device uses the difference of two measurements to calculate the envelope volume of the sample. A specific medium (DryFlo™) is used, which is, according to the manufacturer (Micromeritics Instrument Corporation, 2017), a quasi-fluid "*composed of small, rigid spheres having a high degree of flow-ability*", forming a tight packing around the object under examination. The particles are small enough to closely conform to the object's surface during consolidation, without infiltrating the pore space. In a first round of measurement, a plunger must travel a distance m_1 to compact the Dry Flo medium in the sample chamber under rotation (Fig. 3a). To use the device, the samples must be sufficiently consolidated to withstand the mechanical impact of the Dry Flo during compaction. Based on sample chamber sizes, samples with max. dimensions of approximately 58 x 60 x 80 mm (278,4 cm^3) can be used. The rock sample is then added to the cylinder with the Dry Flo and in a second measurement the distance m_2 is measured (Fig. 3b). The envelope volume of the sample, equaling the displacement volume (V), is calculated as

$$V = \pi r^2 d \,, \qquad (1)$$

where r represents the radius of the used sample chamber and d the difference in the traveling distance of the plunger (m_1-m_2; Fig. 3) (Micromeritics Instrument Corporation, 2016, 2017).

https://doi.org/10.5194/egusphere-2026-3450
Preprint. Discussion started: 7 August 2026

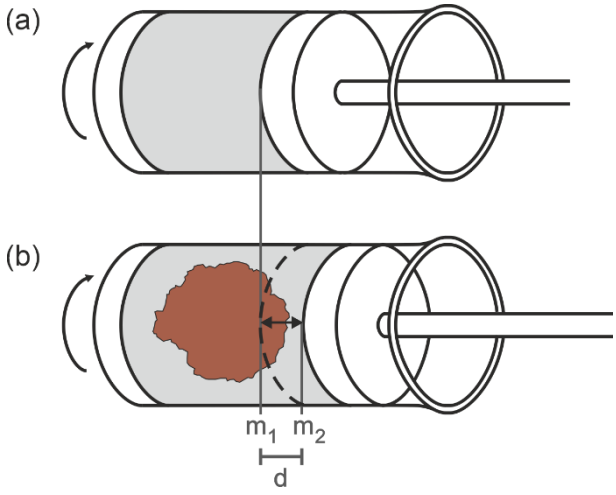

Figure 3: Travelled distance of the plunger m_1 recording (a) only the consolidated Dry Flo medium and (b) m_2 after the rock sample has been added to the Dry Flo medium (redrawn after Micromeritics Instrument Corporation, 2016).

According to the operator manual (Micromeritics Instrument Corporation, 2017) the chosen sample chamber volumes should be filled with at least 25 Vol.% of the sample and 75 Vol.% of Dry Flo, preferably. In order to approach this ratio the smallest sample chamber that can accommodate the selected sample is used (see Appendix C for the used sample chambers). For each measurement ten preparation cycles are carried out so that the beads of the Dry Flo can align regularly to each other and to the surface of the sample during compaction. After ten measurement cycles the average values for the envelope volume [cm^3] (incl. standard deviation) and the sample volume [%] in comparison to the sample chamber volume are calculated. Additionally, by the input of the sample mass through a connected digital scale, the average envelope density [g cm^{-3}] (incl. standard deviation) and corresponding porosity [%] are provided.

Calibration runs, which would account for irregularities of the sample by creating a new conversion factor for the calculation of the volume based on the distance traveled by the plunger, could not be performed. This is because no reference object of known properties, with the same geometry of the sample pieces are available (Micromeritics Instrument Corporation, 2017).

Comparable to the 3D micro-scanner work flow, the following default parameters were selected to assess the reproducibility of the device. The measurements were carried out three times, with ten measurement cycles each, for every rock sample. Additionally, the amount of the sample to Dry Flo volume ratio was kept constant (±1 %) as well as the force with which the plunger compacts the medium. For suitable rock samples, the sample-to-medium ratio was changed to check for a possible influence on the resulting envelope volume. Furthermore, we tested an increase of force that pushes the plunger into the sample chamber, as recommended, if the measured height of the filling (Dry Flo including the sample) exceeds the diameter of the sample chamber (cf. modified setup in Fig. 1).

https://doi.org/10.5194/egusphere-2026-3450
Preprint. Discussion started: 7 August 2026

2.4 Assessment of results

2.4.1 Sample characteristics

To quantify the visual surface characteristics (introduced in the following chapter), the surface roughness (Eq. 2) and the remaining hole area (Eq. 3) were calculated, based on the 3D model. Thereby the surface roughness R_a is described as the ratio of the mean surface area (A_{avg}) and the absolute arithmetic mean envelope volume of a sample (V_{avg}).

$$R_a = \frac{A_{avg}}{V_{avg}}\,, \tag{2}$$

The relative hole area A_h is the average percentual surface area, which could not be captured by the 3D Micro-Scanner, in relation to the average surface area (A_{avg}) of the finished model (Eq. 4).

$$A_h = \left(\frac{A_{avg} - A_S}{A}\right) * 100\,, \tag{3}$$

Whereby A_S denotes the surface area, which could be scanned by the device.

2.4.2 Reproducibility calculation

The reproducibility and accuracy of optical 3D scanners has been addressed before (Mendricky and Sobotka, 2020; Eiríksson et al., 2016), typically according to standards like the Verein Deutscher Ingenieure and Verband der Elektrotechnik Elektronik Informationstechnik (2002) or the more recent Deutsches Institut für Normung (2023). These use a length measurement error of or between defined geometric shapes to estimate the reproducibility of 3D measurement systems. However, due to the limitation of executable measurement cycles caused by variable sample geometries and the partially unstable material we instead used the relative volume error ε_{rel} (Eq. 4) to assess the reproducibility. ε_{rel} refers to the maximum measured volume difference (V_{max}-V_{min}) in relation to the absolute arithmetic mean volume of the sample (V_{avg}):

$$\varepsilon_{rel} = \left(\frac{V_{max} - V_{min}}{V_{avg}}\right) * 100\,, \tag{4}$$

3 Rock samples

A variety of rock samples was selected to cover a broad range of textures and different rock types (sedimentary, igneous, metamorphic; Fig. 4).

The samples, which are described in detail below, have been structured into categories that describe unique surface and shape attributes (Table 1). Because each sample can show two or more of those surface and shape attributes, we refer to the most characteristic one by the symbol “++” in the following. In this context, the category “smooth surface” groups all samples, which show an even surface without visible irregularities (e.g. pores) to the unaided eye. The label “porous” refers to samples with visible pores, which create concave shapes. A “high

https://doi.org/10.5194/egusphere-2026-3450
Preprint. Discussion started: 7 August 2026

surface roughness" addresses surfaces with irregularities, which create deviations from a smooth plane (e.g. due to wall-lining crystals). Samples with a "reflective surface" display crystal planes or a polished surface. "Recessed angles" refer to areas of a sample, which recede strongly for example along bedding planes. An additional tonalite fragment was sawn into a regular cuboid ("geometric shape") to address possible challenges in capturing reflective surfaces during the 3D micro-scan.

Table 1: Shape/surface classification scheme of the analyzed rock samples. The most distinctive surface characteristic is marked by two plus signs (++), additional attributes are noted with one plus sign (+).

Sample	Smooth surface	Porous	High surf. roughness	Reflective surface	Recessed angles	Geometric shape
Conglomerate			+	++		
Sandstone (fine-grained)	++					
Sandstone (coarse-grained)			++	+		
Fossiliferous limestone	++					
Limestone	++					
Dolostone	+	++				
Clayey marlstone	++					
Claystone (laminated)	+				++	
Claystone (isotropic)	++					
Scoria		++	+		+	
Tonalite	+			++		
Tonalite (sawn)	+					++
Serpentinite				++		
Phyllite				+	++	

https://doi.org/10.5194/egusphere-2026-3450
Preprint. Discussion started: 7 August 2026

Figure 4: Tested rock samples and related rock categories. Top row: (a) conglomerate, (b) fine-grained sandstone, (c) coarse-grained sandstone, (d) fossiliferous limestone. Middle row: (e) limestone, (f) dolostone, (g) clayey marlstone, (h) laminated claystone, and (i) isotropic claystone. Bottom row: (j) scoria, (k) tonalite, (l) serpentinite, and (m) phyllite.

3.1 Sedimentary rocks

3.1.1 Conglomerate

The light to dark gray sample (Fig. 4a) is a polymict conglomerate with medium grained gravel. The rock sample shows individual components with a maximal diameter of approx. 15 mm. The clasts consist of limestone, quartz sandstone and quartz. The matrix consists of the same components with a diameter of approx. one to two

https://doi.org/10.5194/egusphere-2026-3450
Preprint. Discussion started: 7 August 2026

millimeters, whereby the cement contains calcite and clay. The sample is inequigranular (bimodal), and the components are well rounded. The latter show a moderate compositional and structural maturity. The rock-sample is grain supported, and isotropic, as well as moderately to well cemented. The convex shape of the well-rounded clasts creates reflective areas, the protruding gravel grains result in a high surface roughness (Table 1).

3.1.2 Fine-grained sandstone

The rock can classifies as Intramicrite (Folk, 1959) or Packstone (Dunham, 1962). The sample (Fig. 4b) is medium gray and contains mostly quartz grains (40–45 %) with diameters of a few micrometers up to approx. 200 µm. The grain shapes are dominantly elongated, individual grains show sizes of >300 µm. Carbonate components are micrite grains (peloidal; 25-30 %) and sparite crystals (25-30 %), both showing diameters of >200 µm. Mica particles (<5 %) reach diameters of up to 150 µm. Components are grain-supported and poorly rounded. The sample shows a low compositional and structural maturity and is homogeneous, isotropic and moderately cemented. Due to the small grain size of the calcareous sandstone only minor surface roughness and thus smooth surface are common (Table 1).

3.1.3 Coarse-grained sandstone

The sample (Fig. 4c) classifies as Sublitharenite (Pettijohn et al., 1987). The sample shows a light grey to bluish green color. Quartz is the major component (85-90 %), ranging in size from a few micrometers up to one millimeter; only few grains reach sizes >3 mm. Calcite (5-10 %) is present as micrite and as sparite crystals, with up to 600 µm diameter. Individual crystals reach sizes of >2 mm. Glauconite (<5 %) shows a grain size of approx. 300 µm. The sample is poorly sorted and grain-supported, all components are poorly rounded. It is poorly cemented and characterized by a homogeneous and isotropic fabric. Its high surface roughness is caused by the rocks grain size. Additionally, some components are large enough to show reflecting crystal planes (Table 1).

3.1.4 Fossiliferous limestone

The sample (Fig. 4d) classifies as Biomicrudite (Folk, 1959) or Rudstone (Dunham, 1962), in southern Germany this type of rock is known as “Rosenheimer Kalkstein” (Grimm and Koch, 1990). This sample is characterized by 50-60 % calcareous fossil fragments, mainly of the red algae *Lithothamnium calcareum* with up to 5 mm diameter besides a few crinoid stem limbs. It also contains 5-10% moderately rounded quartz-grains and accessory black lithoclasts, both with ≤1 mm diameter. The sample is polymodal, whereby the majority of the grains are poorly rounded, which indicates a low structural maturity. The sample is grain-supported and anisotropic. Besides the red algae, some of the fossils could be identified as stem limbs of crinoids. The rock is strongly cemented.

https://doi.org/10.5194/egusphere-2026-3450
Preprint. Discussion started: 7 August 2026

Although the sedimentary rock shows small details in the form of fossil fragments, in general the surface is very smooth (Table 1).

3.1.5 Limestone

The sample (Fig. 4e) classifies as Fossiliferous Micrite (Folk, 1959) or Mudstone (Dunham, 1962). The beige micrite matrix dominated sample is poorly sorted and matrix-supported, due to the presence of 5-10% randomly distributed fossil fragments, reaching up to 5 mm grain size. It is well lithified and isotropic, tending to create smooth, but non-planar fracture surfaces (Table 1).

3.1.6 Dolostone

The rock sample (Fig. 4f) classifies as fine-grained Dolomite (dolostone) (Folk, 1959) or Grainstone (Dunham, 1962). It is isotropic and well cemented. It is well sorted, contains no micrite and is completely made up of grain supported, ca. 1 mm sized dolomite crystals. Characteristic features are abundant, irregularly shaped cavities with up to several millimeters diameter and euhedral wall-lining dolomite crystals. The rock sample is classified as dolostone or fine-grained dolomite *sensu* Folk (1959) or grainstone (Dunham, 1962). Generally, the components and fabrics of the rock sample favour smooth rock surfaces, which are however interspersed by large pores (Table 1).

3.1.7 Clayey marlstone

The rock sample (Fig. 4g) can be classified as clayey marlstone. The sample has a brownish grey color and is anisotropic. The bedding is indicated due to the varying relief of the sedimentary layers on the fractured surfaces. The sample is well compacted and its small grain sizes create smooth rock surfaces. Recessed angles are present perpendicular to the bedding planes. However as the thin layers are laminated, the recessing areas are rather small (Table 1).

3.1.8 Laminated claystone

The sedimentary rock (Fig. 4h) classifies as claystone (ger. “Opalinuston”, South German and Swiss Jurassic Lithostratigraphic unit). The dark gray sample is anisotropic due to foliation. Although no particles easily crumble off, they can be removed by only moderate mechanical impact. The smooth rock surface is likely due to the small grain-size, however the recessed angles perpendicular to the bedding planes are significantly more pronounced than those of the clayey marlstone (Table 1)

https://doi.org/10.5194/egusphere-2026-3450
Preprint. Discussion started: 7 August 2026

3.1.9 Isotropic claystone

The sample (Fig. 4i) can be classified as claystone ("Bentonite"). The light beige sample shows no macroscopic visible grains. The sample is isotropic, well compacted and sensitive to mechanical impact. Heating above 50°C leads to fracture formation due to shrinking. The small and uniform grain sizes of the sample create a very smooth rock surface (Table 1).

3.2 Igneous rocks

3.2.1 Scoria

The igneous rock (Fig. 4j) classifies as basaltic scoria lapillus. It has a highly irregular shape and an isotropic texture. It is characterized by high vesicularity, comprising numerous variably sized cavities, resulting from trapped gas bubbles. The sample is permeated by pores of different sizes, which even create recessed angles and a high surface roughness (Table 1).

3.2.2 Tonalite

The sample (Fig. 4k) classifies as Tonalite (Streckeisen, 1974). The leucocratic, light gray sample is medium-grained, equigranular and holocrystalline with an isotropic, compact texture typical of a plutonic origin. Due to its phaneritic texture main components can be macroscopically identified as quartz (30-35 %), biotite (10-15 %), and plagioclase (50-55 %), the latter reaching grain sizes up to 5 mm. While the grain size allows to create smooth surfaces, well developed cleavage planes of the prevailing feldspar components are highly reflective (Table 1).

3.3 Metamorphic rocks

3.3.1 Serpentinite

The dark green serpentinite sample (Fig. 4l) is finegrained, equigranular and anisotropic, due to an obvious metamorphic foliation. It is dominated by phyllosilicates such as chrysotile, antigorite and lizardite; besides few altered olivine crystals. The polished surfaces, caused by slickensides along shear planes create reflecting areas (Table 1).

3.3.2 Phyllite

The metamorphic rock (Fig. 4m) classifies as Phyllite. It is medium gray, with a greenish-silver luster. As individual grains, white mica, chlorite and small amounts of feldspar and quartz are identified. The sample is fine to medium-grained and heteroblastic with a lepidoblastic texture. Its anisotropic fabric is mirrored by the presence of subparallel schistosity planes. The polished surface of the metamorphic rock only shows a silky luster, thus the

https://doi.org/10.5194/egusphere-2026-3450
Preprint. Discussion started: 7 August 2026

reflecting habit is not as prominent as for the serpentinite. However, recessed angles are noticed perpendicular to the schistosity planes (Table 1).

4 Results

4.1 3D Micro-scan

4.1.1 Handling experience

An envelope volume measurement using optical 3D micro-scanning involves a) fixing the sample in the vice in different positions to allow a full coverage of the sample surface during the scans, b) editing and c) fusing the 3D point cloud to a seamless 3D volume with a closed surface. Hereby, fixing the samples in the vice requires skill and caution to avoid damage or the sample falling out during the scan. Hard-to-reach or reflective crystal areas can be captured by adjusting the number of individual frames for each scan, the scan number during each step of the processing workflow and by mounting the sample at different angles.

Depending on the extent of the corrections after the actual scan, the overall time for the entire measurement procedure takes 10-15 minutes. Changing the settings of the measurement procedure such as the scan path or the fusion of scans has a minor influence on the resulting volumes (≤0.56 % deviation out of three measurements; see Appendix C for the measured values), although it leads to a longer time period needed to complete the measurement.

Changing the scan path (from “small normal” to “small simple”) has no influence on the resulting volume, but is reducing the frame sizes, and thus the angles in which the samples are recorded, which in turn can lead to more “holes” in the scanned surface. By changing the fusion types (“fast fusion” to “sharp fusion”), no general trends regarding a systematic increase or decrease of the resulting volumes were observed. Differences of the mean volume values of the individual scans may vary up to 0,51 % of the total volume (e.g., dolostone), whereby the “sharp fusion” does not show a smaller relative error in general. The elapsed time for the calculation of the different fusion types seems to depend on the computing power but in general is significantly higher for the “sharp fusion” (up to 15 min.) compared to “fast fusion” (usually <60 sec.).

4.1.2 Suitability for rock samples

The main challenge for optical 3D micro-scanning is approaching full coverage of the sample surface resulting in a minimum of holes in the digital representation of the sample. The scan coverage , however, highly depends on the sample’s surface and shape attributes (Fig. 5). Good scan coverage resulting only in a few holes in the modelled sample surface and thus good reproducibility can be expected if the surface of the sample is smooth and displays a low surface roughness (e.g. clayey marlstone, fine-grained sandstone, fossiliferous limestone,

https://doi.org/10.5194/egusphere-2026-3450
Preprint. Discussion started: 7 August 2026

isotropic claystone, laminated claystone, laminated claystone, limestone, sawn tonalite). In contrast, large pores (e.g. dolostone, scoria), recessed angles (e.g. laminated claystone, phyllite), and a high surface roughness (e.g. coarse-grained sandstone) can result in incomplete scan coverage and larger holes. Shapes with sharp edges (isotropic claystone, sawn tonalite) can also lead to small holes, presumably due to translucent crystals. Samples whose surface is characterized by reflective minerals (tonalite) or a reflective appearance due to a polished surface or convex shapes (serpentinite, rounded components in the conglomerate) are prone to a larger number of holes in the samples surface coverage.

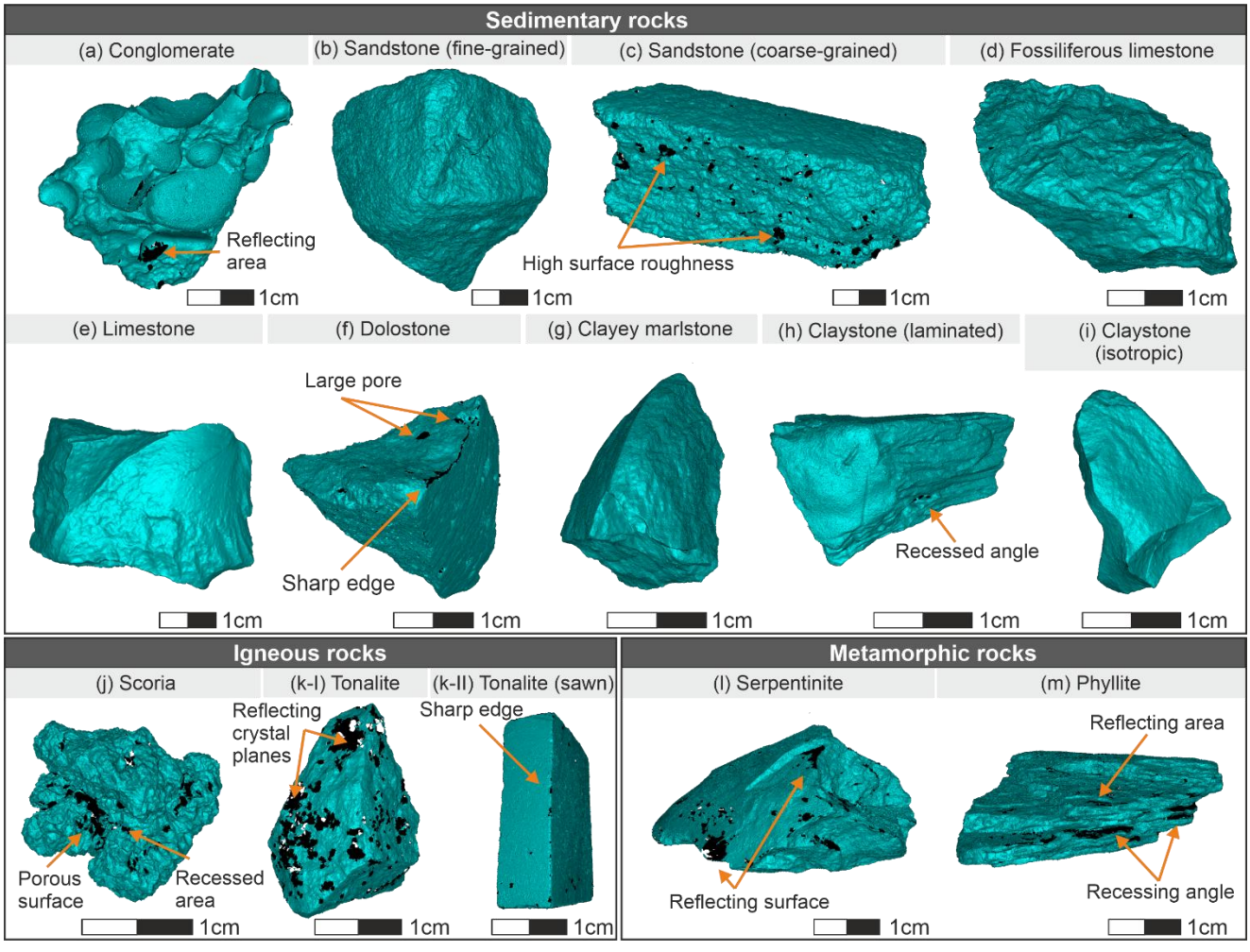

Figure 5: Aligned and merged 3D-scans of the examined rock samples. Holes are either visible by the background color or are shown in black when there is a closed surface in the background. Note the sizes and amounts of holes in areas with reflecting mineral cleavage planes (tonalite) or polished surfaces (serpentinite), recessed angles (laminated claystone, phyllite), big pores (dolostone, scoria) and a high surface roughness (coarse-grained sandstone).

https://doi.org/10.5194/egusphere-2026-3450
Preprint. Discussion started: 7 August 2026

4.1.3 Processing

The final 3D surfaces of the rock samples with filled holes, displayed in Fig. 6, are used for the volume calculation. Small holes created at edges or convex surface shapes show a realistic surface after the automatic hole filling, when compared to the original sample outlines.

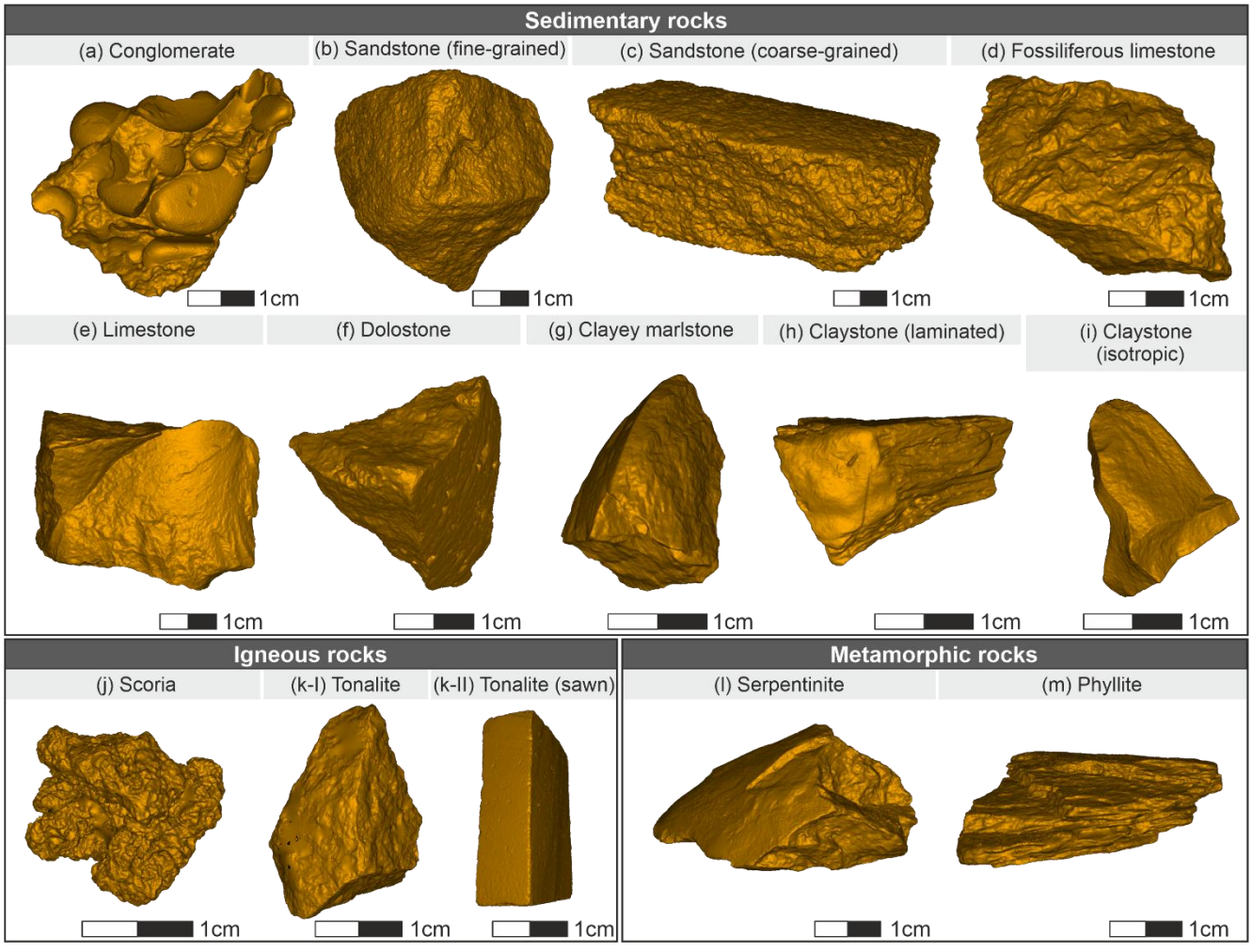

Figure 6: Final surfaces of the 3D-scanned rock samples with filled holes after processing.

Larger holes, as observed in the tonalite, lapilli and dolostone models require first a manual filling (“fix holes”) to avoid unrealistic geometries generated by the following automatic “hole filling” process. Where the area which cannot be captured by the camera is too large, as for example in a section of the tonalite model (Fig. 7), isolated pieces, which could be captured by the camera, are not incorporated into the meshed surface by the algorithm. The resulting surface thus is smaller than that of the actual sample.

https://doi.org/10.5194/egusphere-2026-3450
Preprint. Discussion started: 7 August 2026

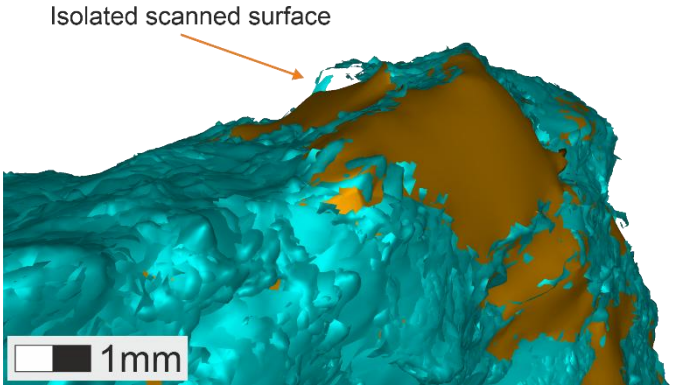

Figure 7: Side view of scanned fragments (turquoise), which are not incorporated into the meshed surface (orange) of the sample (tonalite) by the algorithm.

The scoria and the dolostone samples show recessing areas due to the presence of pores, which are hard to capture by the projected light. The meshed areas follow the recessing, concave surface, but sometimes do not represent exactly the correct original sample shapes or complex geometries (Fig. 8). Similar observations are noticed in the case of large recessing angles due to bedding.

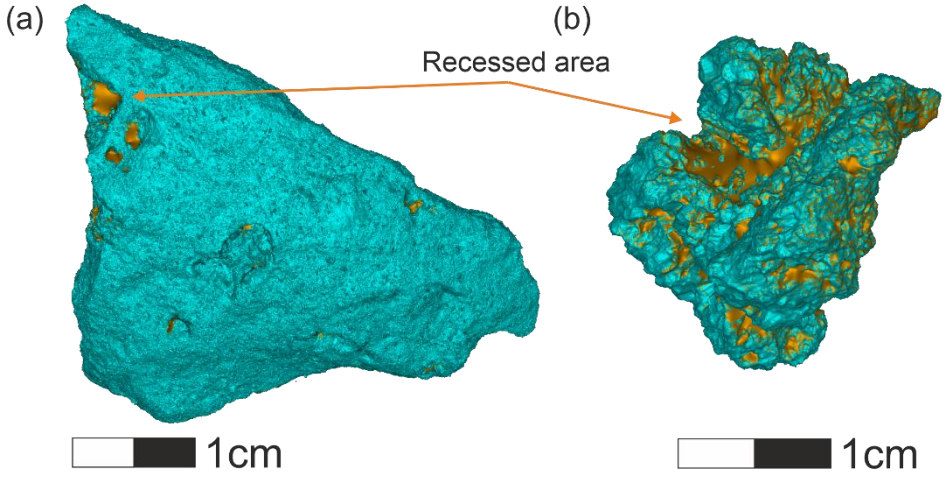

Figure 8: Scanned surface (turquoise) and the meshed hole filling (orange) of (a) the dolostone and (b) the scoria sample. Notice that the recessed areas of the samples are filled by a meshed, smooth surface approximation.

4.2 Envelope density analyzer

4.2.1 Handling experience

The handling of samples in the course of the measurement with the density analyzer is accompanied by a few issues. Occasionally, individual crystal or rock fragments detach during the measurement. Especially with very porous rocks, such as the dolostone and the scoria, a fraction of the Dry Flo medium adheres to the samples. Dry Flo also sticks to hands and tools (brush).The handling of the Dry Flo, especially when the sample is inserted into

https://doi.org/10.5194/egusphere-2026-3450
Preprint. Discussion started: 7 August 2026

the sample chamber, has to be taken with care, because losses of Dry Flo will result in a decrease of the inferred envelope volume of the sample. Considering both the time for preparation and the measurements, one analysis takes about 20 minutes.

4.2.2 Suitability for rock samples

A volume ratio of at least 20–25 % for the sample to 75–80 % of Dry Flo could not be realized in most cases, due to the irregularly shaped geometries of the rock samples. According to the manual, one should avoid reducing the sample volume below ten percent of the total sample chamber volume, which could not be realized for the conglomerate and the tonalite sample. When the sample measurement is carried out with an insufficient amount of Dry Flo, particles are visibly moving through the narrow space between plunger and sample chamber walls, while the sample is clamped between the ends of the sample chamber.

Two different approaches were tested to reduce the error resulting from this issue. First, different orientations of the samples in the sample chamber were tested, minimizing the necessary amount of Dry Flo to cover the whole rock specimen. However, when installing the sample chamber to the device, the rotation of the chamber at the onset of compression by the plunger allows the sample to move in orientation and eventually clamp between the glass and the plunger.

The second approach ensures a sufficient volume of Dry Flo to completely embed the rock specimen, regardless of its orientation. In this case the medium exceeds the recommended share of the complete infill (<80 %). We tested to increase the force with which the plunger compacts the sample chamber fill, as is also suggested in the case the height of the infill exceeds the diameter of the sample chamber (Micromeritics Instrument Corporation, 2017). However, this approach shows no significant change in the resulting envelope volumes. Additionally, this could not be realized for very fragile samples. Instead, general observations and measurements using different amounts of the Dry Flo medium were analyzed to quantify the deviation in the resulting envelope volumes (Fig. 9). It is noticeable that a decreasing portion of Dry Flo leads to a significant increase in the measured envelope volume of the sample. The measurements show that a one-percent change in the ratio of the sample to Dry Flo can potentially increase the envelope volume up to eight percent. This effect, however, flattens for samples with a smooth surface. For example, for an aluminum cylinder (avg. envelope volume: 28244.70 mm^3) the effect of the increasing envelope volume with a decreasing share of the Dry Flo is not evident and instead the values remain constant (Fig. 9). It is therefore presumed that the increase in the envelope volume flattens for materials with decreasing irregularities on the surface of the sample. The data show that samples with major inhomogeneities such as larger pores and rocks with a high surface roughness are affected.

https://doi.org/10.5194/egusphere-2026-3450
Preprint. Discussion started: 7 August 2026

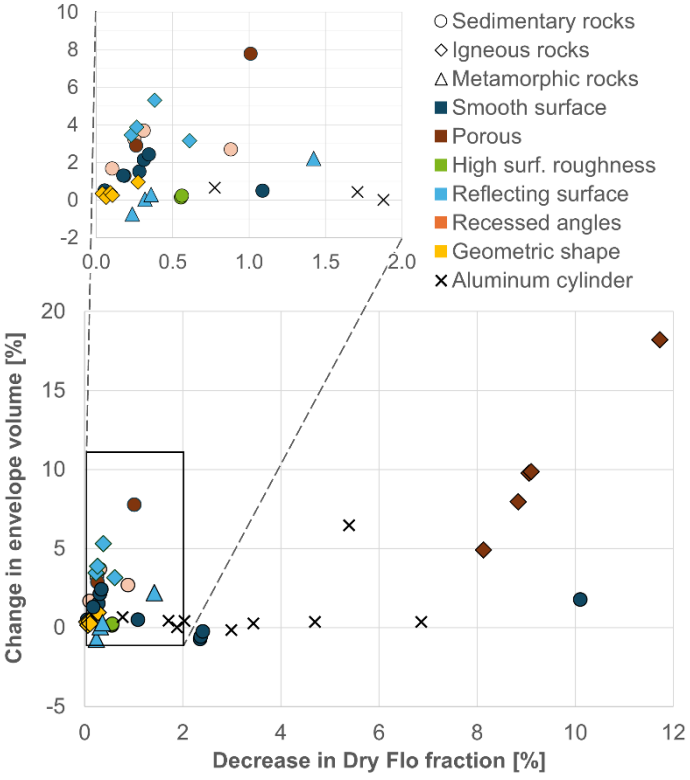

Figure 9: Envelope density analyzer measurements using different amounts of the Dry Flo medium and the same rock sample to quantify the deviation in the resulting envelope volumes. Standard rock samples show a mostly positive change in the sample volume after increasing the ratio of the sample to the Dry Flo, whereas this effect seems to flatten for samples with a smooth surface. The black crosses depict the same measurement approach using an aluminum cylinder.

4.3 Envelope volume: 3D Micro-scanning vs. envelope density analysis

A comparison of the absolute envelope volumes for measurements with the same default parameters for both 3D micro-scanning and envelope density analysis is shown in Fig. 10 (see Appendix C for the measured values). Depending on the sample type, the absolute envelope volumes determined using the 3D micro-scanner show a minimal difference of 0.74 mm^3 (clayey marlstone, avg. envelope volume: 2917.30 mm^3) and a maximal difference of 99.71 mm^3 (dolostone, avg. envelope volume: 6289.60 mm^3) out of three measurements. The values determined with the envelope density analyzer vary between 5.50 mm^3 (isotropic claystone, avg. envelope volume: 8375.50 mm^3) and 484.40 mm^3 (dolostone, avg. envelope volume: 6289.60 mm^3). The relative errors resulting from the envelope density analyzer measurements (0.23–7.55 %) exceed those calculated using the 3D micro-scanner (0.02–1.59 %), except for the coarse grained sandstone (3D micro-scanner: 0,43 %; Envelope density analyzer: 0,23 %). It is apparent that rock samples, which exhibited difficulties during the measurement (3D micro-scanner: correct representation of the surface; Envelope density analyzer: residues of the dry-fluid

https://doi.org/10.5194/egusphere-2026-3450
Preprint. Discussion started: 7 August 2026

medium in the sample) are characterized by high relative errors. Notably, samples with large pores (dolostone, scoria) or a high surface roughness (coarse-grained sandstone) lead to a larger variation of the envelope volumes, determined with the 3D micro-scanner. Recessed angles and reflecting surfaces require additional scan runs to depict the surfaces correctly, but do not show a high variability in the measured volumes. The regular shape of the sawn tonalite sample creates difficulties in aligning the individual scans. Samples with a smooth surface (fine-grained sandstone, fossiliferous limestone, limestone, clayey marlstone, isotropic claystone) are expected to yield highly reproducible results. Large pores, recessed angles (laminated claystone, phyllite) and increased roughness of a sample's surface also appear to negatively influence the measurements taken by the envelope density analyzer, whereas reflective surfaces have no effect whatsoever.

With exception of the laminated claystone, scoria and clayey marlstone, all other mean envelope volumes determined with the 3D micro-scanner exceed those taken by the envelope density analyzer (Fig. 10). The differences in envelope volumes, calculated for the mean values acquired with the 3D micro-scanner and the envelope density analyzer range between -199.35 mm³ (laminated claystone) and 272.33 mm³ (sawn tonalite).

Overall, the absolute volumes measured by the 3D micro-scanner and the absolute volumes derived by the envelope density analyzer indicate a good correlation (Fig. 11a). This picture changes completely when the relative error is used as an indicator of reproducibility of each method: Relative to the mean envelope volume, the maximum relative error of the 3D micro-scanner is lower for all tested rock samples compared to the envelope density analyzer (Fig. 11b). The isotropic claystone and the sawn tonalite sample exhibit approximately equal relative errors for both devices. Both, the porous surface of the dolostone and of the scoria exert the greatest influence on the envelope volumes which were measured using the 3D micro-scanner and the envelope density analyzer.

https://doi.org/10.5194/egusphere-2026-3450
Preprint. Discussion started: 7 August 2026

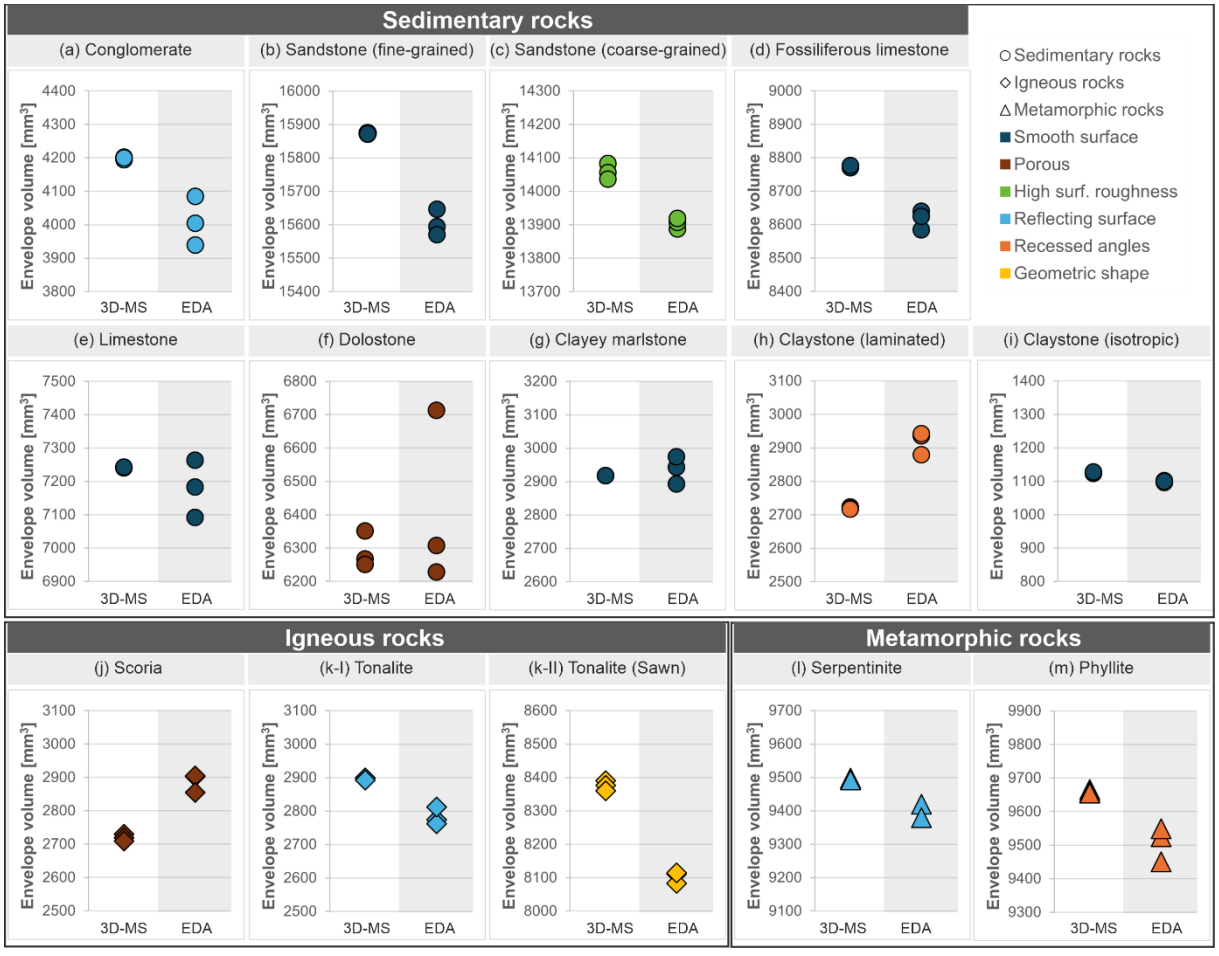

Figure 10: Comparison of the calculated envelope volumes (mm³) for the tested rock samples based on measurements using a 3D micro-scanner (3D-MS) and an envelope density analyzer (EDA). Note that the type of ornament refers to the rock type, whereas the color refers to the shape/surface classification of the respective rock sample (see Tab. 1).

https://doi.org/10.5194/egusphere-2026-3450
Preprint. Discussion started: 7 August 2026

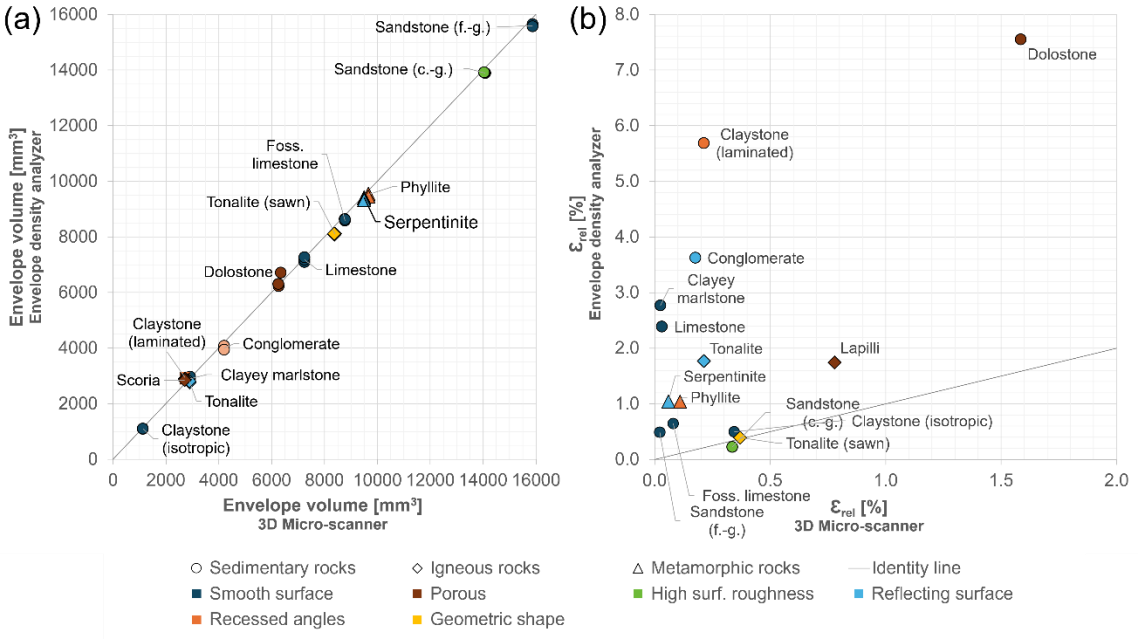

Figure 11: (a) Absolute envelope volumes (mm³) determined by the 3D scanning method compared to the volumes acquired by the envelope density analyzer, indicating a good correlation between the two measurements. (B) Comparison of relative errors in measurements using the 3D micro-scanner and the envelope density analyzer. Note that relative to the mean envelope volume, the maximum relative error of the 3D micro-scanner is lower for all tested rock samples compared to the envelope density analyzer The colors indicate the main surface characteristic of the respective sample (cf. Table 1). The gray line acts as the identity line.

The relative errors tend to increase proportionally to the surface roughness of the rock samples (red ellipse in Fig. 12) for both, the measurements with the 3D micro-scanner (Fig. 12a) and with the envelope density analyzer (Fig. 12b). Furthermore, the influence of the relative hole area A_h, the average percentage of the surface area that could not be captured by the 3D Micro-Scanner, relative to the average surface area A of the finished model (Eq. 4) requires closer examination. The dolostone (A_h: 3.35 %), the scoria (A_h: 10.29 %), the sawn tonalite (A_h: 2.82 %) and the coarse grained sandstone (A_h: 8.62 %) all show a relative error higher than the overall relative error trend for the 3D micro-scanner, which is attributed to the incorrect meshing of the hole area or alignment (sawn tonalite) respectively. Although the tonalite (A_h: 26.08 %) and the serpentinite (A_h: 10.77 %) scans have the largest hole area in comparison to the watertight models, the results show a rather low relative error. This is due to the hole area consisting of a plane surface, which is depicted accurately by the meshing tool.

For the envelope density analyzer, the dolomite and the laminated claystone have a higher relative error than the average trend in relation to the surface roughness. This might be related to the recessing angles and pores, preventing a uniform arrangement of the rigid spheres of the Dry Flo medium around the sample.

https://doi.org/10.5194/egusphere-2026-3450
Preprint. Discussion started: 7 August 2026

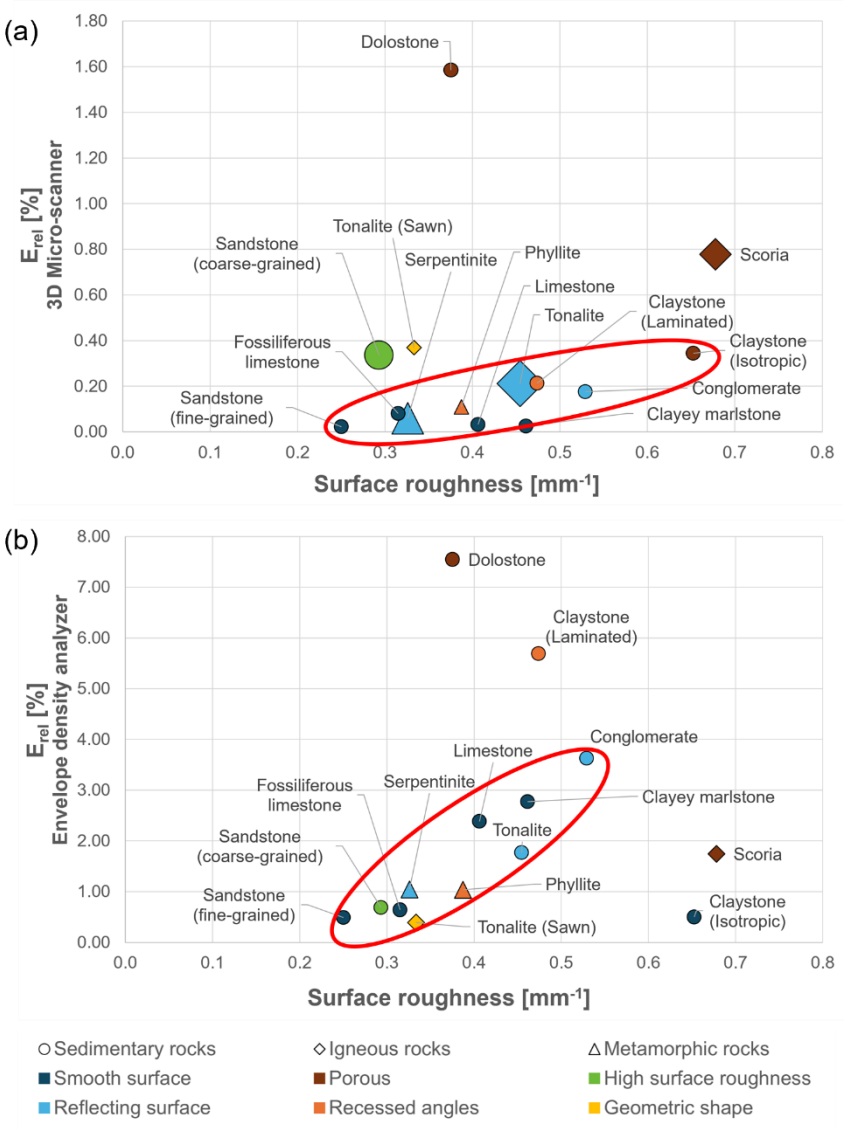

Figure 12: Mean relative errors of the samples with respect to their surface roughness for the measurements using (A) the 3D micro-scanner and (B) the envelope density analyzer. The symbol size in (A) indicates the remaining hole area, the surface area which could not be captured by the 3D Micro-Scanner (small: <5 %, medium: 5 % ≥ Ah <20 %, large: ≥20 %). The diagrams show upward trends of the relative error, which is proportional to the surface roughness of the samples for both, the 3D micro scanner and the envelope density analyzer. An exceptional big hole area leads to a disproportional increase of the relative error, especially if the missing surface shows a complex geometry and therefore an often incorrect representation by the meshing tool.

https://doi.org/10.5194/egusphere-2026-3450
Preprint. Discussion started: 7 August 2026

5 Discussion

The decision whether optical 3D micro-scanning is suitable for the determination of the envelope volume of a rock sample relies mainly on the ability to capture (a) characteristics of the samples as a three-dimensional model, (b) the reproducibility, and (c) the accuracy of available devices.

5.1 Effects of sample characteristics

Different surface properties of the sample can strongly influence the suitability of 3D micro-scanning for creating a reliable three-dimensional model. Table 2 summarizes the various surface properties and recommends corresponding adjustments to the measurement procedure. As with the envelope density analyzer large pores and recessed angles also lead to inaccurate measurements using the 3D micro-scanner. Such areas that cannot be fully reached by the light beam lead to holes in the 3D model. Polished and reflective surfaces (e.g. due to large crystals) that scatter or reflect the light beam lead to the same disadvantage. While flat surfaces such as large crystal or crystal cleavage planes, can be properly depicted by meshing, concave or more complex shapes such as pores, can be cut off and thus can enlarge the actual sample volume.

Preparing the sample by sawing is not necessary. However, it supports the otherwise non-invasive optical scanner to picture object points uniformly over the whole sample, because the occurrence of cleavage planes (e.g. feldspar) and fractured surfaces (e.g. quartz) on the samples surface (e.g. tonalite) can be avoided. However, this approach can also result in deviating envelope volumes because sharp edges cannot be depicted entirely. Individual scans may not be aligned correctly due to the lack of characteristic marker points, therefore it is recommended to cut off one edge of the sawn Euclidean geometry (e.g. cuboid). Good depictions can be expected from areas with a smooth surface, as common for chemical sedimentary rocks, resulting from small grain sizes (approx. ≤0.2 mm, medium grained sand after Deutsches Institut für Normung, 2020) in clastic sedimentary rocks, for sawn surfaces of well-cemented sedimentary rocks, or for igneous and metamorphic rocks. The dark color of some rock samples does not create difficulties due to the adjustable brightness.

Table 2: Assessment and recommendations for the use of an optical 3D micro-scanner regarding different rock properties and rock surface characteristics.

Surface characteristics	Assessment/Recommendations
Smooth surface, low surface roughness	Highly reproducible results
High surface roughness	Deviating scans possible Recommendation: cut the sample into shape provided it is sufficiently consolidated/lithified

https://doi.org/10.5194/egusphere-2026-3450
Preprint. Discussion started: 7 August 2026

Large pores	Deviating scans possible Recommendation: use multiple scan paths, use manual hole filling
Recessed angles (e.g. bedding)	Deviating scans possible Recommendation: careful sample selection or preparation, use multiple scan paths
Reflective surfaces (e.g. crystal planes)	Deviating scans possible Recommendation: use multiple scan paths or cut the sample into shape
Simple geometries	Potential difficulties in aligning the scans Recommendation: for samples with predominant share of reflective surfaces
Lithification	Careful handling enables measurement of poorly lithified or bizar shaped rock samples without parts of the sample breaking off

5.2 Handling, reproducibility and accuracy

The reproducibility of the determined envelope volumes tends to be strongly influenced by the surface properties of the measured rock sample (Fig. 11b, 12). Deviations occur primarily due to large holes in the scanned surface, suggesting that the resulting errors stem essentially from differing solutions for the meshed surface. Nevertheless, the optical 3D micro-scanner generally exhibits significantly lower scatter in the determined envelope volumes and thus higher reproducibility (relative error ≤1,59 %) than the envelope density analyzer (relative error ≤7,55 %;Table 3). For both devices the surface roughness can serve as an indicator of the quality of the results. Although this is masked by the quality of the meshing process for holes in the scans, it can be assumed that the relative measurement error increases in proportion to the surface roughness of the rock sample. A direct comparison of the relative error with similar studies is not possible due to the limited availability of comparable investigations that provide specific values regarding device reproducibility. However, Weydt et al. (2021) compiled a database of mechanical and petrophysical rock properties, which also includes values for the porosities of limestone and pyroclastic rocks. To analyze the bulk volume of their samples they employed the triple weighing method after Brown (1981), the caliper method according to ASTM International (2016) and the GeoPyk (Micromeritics Instrument Corporation, 1998). The study reports a coefficient of variation for bulk and raw densities between the different measuring methods of 0,5-3.5 % for pyroclastic rocks (porosity 11-15 %) and 0,3-3,0 % for limestones (porosity ≤3 %). To put the values obtained via the optical approach into proper perspective, it can be noted that the coefficient of variation (≙ mean variation) of the values across the devices

https://doi.org/10.5194/egusphere-2026-3450
Preprint. Discussion started: 7 August 2026

falls within a range similar, or even exceeds, the reproducibility (relative error ≙ maximal variation) of the 3D micro-scanner.

While industry measurements depend to a significant extent on the accuracy of the device, in the present application, the capture of complex geometries also plays a decisive role in achieving the most precise volumes possible. The accuracy of the scanner used depends on the correct assignment of specific points (pinpoint accuracy ≥0.01 mm; Artec 3D, 2020) as well on the meshing procedure. In terms of the resolution, two points separated by a distance of 0,029 mm can be distinguished. This spacing between two adjacent points is sufficiently small to resolve the grain size of sand in accordance with Deutsches Institut für Normung (2020). However, although components with a grain size falling within a range similar to the resolution, such as coarse-grained sandstone, can be detected by the device, accurately rendering the grain shape proves challenging. Consequently, the scanner generates individual scans based on distinct points on the sample surface, which leads to greater deviations in the merged models and, as a result, to a higher relative error. In contrast, the surfaces of samples with finer grain sizes can be mapped with precision. This is attributable to the low surface roughness, where the average surface (fusion-model), derived from two or more individual scans, does not compromise the geometric form of the sufficiently planar surfaces.

The envelope volume is a prerequisite for the measurement or derivation of bulk density and porosity, both parameters that are of crucial importance in geophysics and in the extraction of fluids from the subsurface (e.g. Bjørlykke, 2015), as well as general studies, such as those addressing the geological evolution of sedimentary basins (Allen and Allen, 2013). Since porosity is a function of the ratio between the skeletal volume and the envelope volume, the impact of potentially incorrectly measured envelope volumes is particularly high for rock samples with low porosity. Consider, for example a rock sample with a skeletal volume of 1 cm^3 and an actual porosity of 5 % would result in a calculated porosity of 9.5 % if the measured envelope volume deviates by 5 % from the actual envelope volume. Therefore, envelope volumes should be determined several times and with high reproducibility, especially where low porosity is to be expected, and if the sample surface is difficult to image.

Beside the device-dependent influencing factors, a largely error-free application is required to ensure reliable results. This is ensured by the optical device due to its intuitive handling as well as the ability to add additional scans at every stage of the processing. Compared to other techniques, including the envelope density analyzer, the fully automated approach of a 3D micro-scanner exhibits a reduced influence of the user on the reproducibility or even accuracy. The precision of measuring the dimensions of an Euclidean geometry relies directly on the operator, by using immersion weighing (Deutsches Institut für Normung, 2007) or mercury porosimetry (Deutsches Institut für Normung, 2019) the samples undergoes several processing steps which are subject to individual interpretation. While the approach using the envelope density analyzer depends on delicate sample handling between two measurements, the optical approach only relies on the proper attachment of the

https://doi.org/10.5194/egusphere-2026-3450
Preprint. Discussion started: 7 August 2026

rock specimen, without interference to the measurement procedure itself. Furthermore a direct comparison reveals that the optical method exhibits a lower susceptibility to errors resulting from material loss during the measurement, a circumstance that can be attributed to the failure detectable during the scanning process. Further advantages include the short measurement duration and training time and the ease of use, as well as additional application possibilities, such as the ability to export the 3D model or analyze the surface structure of samples (Table 3).

In summary, optical 3D micro-scanning is a non-destructive, rapid method for determining the bulk volume of rock samples, which, despite challenges with certain surface properties, produces reproducible results.

Table 3: Comparison of the optical 3D micro-scanner and the envelope density analyzer regarding the training period and measurement time, as well as the reproducibility of the devices and additional advantages.

Criterion	3D micro-scanner	Envelope density analyzer
Familiarization period	~20 min	~60 min
Measurement time	10–15 min	~20 min
Handling	Intuitive Fully automatic Flexible measurements	Familiarity with the device required Cautious handling needed
Reproducibility, relative error	≤1.59 %[a]	≤7.55 %[a]
Advantages	Export options for 3D model Post-editing possible Additional applications (e.g. analysis of surface roughness)	Direct density output possible

a based on the tested rock samples

6 Conclusion

The objective of this study was to evaluate the suitability of an optical 3D micro-scanner for determining the envelope volume of rock samples. Therefore, a selection of sedimentary, igneous and metamorphic rock samples was measured, using an optical 3D micro-scanner and compared with the results of an envelope density analyzer, which is the current industry standard. The results were assessed based on their suitability for capturing various rock characteristics, as well as the reproducibility of the measurements. A key factor influencing the quality of the measured envelope volume is the surface roughness of the rock, with an increase in roughness resulting in a lower reproducibility of the results.

https://doi.org/10.5194/egusphere-2026-3450
Preprint. Discussion started: 7 August 2026

Optical 3D micro-scanning is deemed sufficiently reliable for determining the envelope volume of rock samples based on:

- the high reproducibility of the measurements in compared to the widely used envelope density analyzer.
- accuracy sufficient to characterize the grain size of sand in accordance with DIN EN ISO 14688-1.
- effective capture of smooth surfaces on rock samples composed of pelitic-sized constituents.

Certain adjustments, such as performing additional scans, careful sample selection or trimming may be necessary for samples exhibiting:

- high surface roughness
- large pores or recessed angles
- glossy surfaces

Overall, optical 3D micro-scanning is evaluated as a novel, non-destructive alternative for determining the envelope volume of rock samples, offering rapid results, a user-friendly operation, and potential for application in additional fields.

Appendices

Appendix A: Specifications for the Artec Micro 3D-scanner (Artec 3D, 2020)

Specification	Value
Max. object size	90 x 60 x 90 mm
Rotation module	Biaxial rotation system (panning and rotation)
3D-Pinpoint-accuracy	Up to 0.01 mm (10 µm)
3D-resolution	Up to 0.029 mm
Scanner-Type	Desktop
Recording of textures	yes
Texture-resolution	6.4 mp
Colors	24 bpp
Data acquisition speed	Up to 1 Mio. Points s^{-1}
3D-Exposure time	adjustable
2D-Exposure time	adjustable
Source of light	blue LED
Cameras	two-color cameras
Interface	USB 3.9
Supported operating systems	Windows 10 x64

https://doi.org/10.5194/egusphere-2026-3450
Preprint. Discussion started: 7 August 2026

Recommended processing power	Intel Core i7 or i9, 64+ GB RAM, NVIDIA GPU min. 3 GB VRAM, CUDA 3.5+
Measurements (H x L x B)	290 x 290 x 340 mm
Weight	12 kg
3D-Polygon mesh	OBJ, PLY, WRL, STL, AOP, ASC, Disney PTX (PTEX), E57, XYZRGB
CAD-Formats	STEP, IGES, X_T
Formats for measurements	CSV, DXF, XML
Website	www.artec3d.com

Appendix B: Specifications for the Micromeritics GeoPyc (Micromeritics Instrument Corporation, 2017)

Specification		Value
Frequency		50–60 Hz
Apparent power		175 VA max.
Voltage		100–240 VAC
Temperature		Stable, 15 to 35 °C operating; 0 to 50 °C non-operating
Humidity		20 to 80 % relative (non-condensing)
Exposed Materials; to sample		Glass, graphite, Teflon®, stainless steel, aluminum, Buna-N, epoxy, ceramic
Sample chamber dimensions		
No.	Diameter x length [mm]	Inner envelope volume best measured [cm^3]
1	12.7 x 19.00	0.3–0.8
2	19.1 x 28.00	0.8–2.4
3	25.4 x 38.00	2.4–5.3
4	38.1 x 50.00	5.3–13
5	50.8 x 60.00	13–25
Reproducibility		
Volume sample ≥25 % of the sample chamber		±1.1 %
Device dimensions		
Height		27 cm
Width		55 cm
Depth		38 cm

https://doi.org/10.5194/egusphere-2026-3450
Preprint. Discussion started: 7 August 2026

Weight	16 kg
Medium	Dry Flo

https://doi.org/10.5194/egusphere-2026-3450
Preprint. Discussion started: 7 August 2026

Appendix C: Measured values with the same initial conditions using the 3D micro-scanner (calculated envelope volume, calculated surface area, and surface area with holes) and the envelope density analyzer (volume, standard deviation out of ten measurement cycles).

	3D Micro-scan				Envelope density analysis			
Measurement ID	**Envelope volume**	**Surface area**	**Surface area incl. holes**	**Sample chamber (cf. Appendix B)**	**Envelope volume**	**Standard deviation**	**Ratio sample-to-Dry Flo**
	[mm3]	**[mm²]**	**[mm²]**		**[mm³]**	**[mm³]**	**[%]**
Conglomerate_M1	4194.08	2212.19	2155.84	4	4004.30	17.50	9.59
Conglomerate_M2	4201.46	2224.39	2161.42	4	4084.10	6.80	9.80
Conglomerate_M3	4199.97	2226.46	2138.68	4	3938.70	15.90	9.49
F.-g._sandstone_M1	15873.66	3863.70		5	15594.20	9.20	19.01
F.-g._sandstone_M2	15870.22	3873.00		5	15646.00	13.00	19.05
F.-g._sandstone_M3	15871.00	3875.92		5	15569.70	16.10	18.99
F.-g._sandstone_M4		4034.33	3994.43	5			
F.-g._sandstone_M5		3944.66	3941.62	5			
F.-g._sandstone_M6		3928.63	3923.53	5			
Foss._limestone_M1	8774.40	2766.07	2758.26	4	8583.80	8.90	18.12
Foss._limestone_M2	8769.36	2762.39	2742.83	4	8639.30	27.10	18.24
Foss._limestone_M3	8776.42	2764.27	2741.09	4	8624.50	9.90	18.22
Lamin._claystone_M1	2722.89	1293.89	1291.73	3	2935.60	22.80	23.39
Lamin._claystone_M2	2718.35	1285.17	1281.40	3	2878.60	21.90	22.98
Lamin._claystone_M3	2717.10	1286.42	1284.46	3	2942.20	20.80	23.52
Scoria_M1	2730.04	1853.61	1593.38	3	2902.90	25.60	24.64
Scoria_M2	2718.53	1865.51	1693.72	3	2905.30	22.10	24.69
Scoria_M3	2708.87	1810.62	1673.89	3	2855.00	10.10	24.42
Limestone_M1	7240.05	2935.34	2934.60	4	7091.50	12.90	14.13
Limestone_M2	7240.08	2936.79	2933.54	4	7183.00	11.90	14.31
Limestone_M3	7242.33	2935.91	2948.54	4	7262.90	15.80	14.47
C.-g._sandstone_M1	14083.08	4120.69	3765.29	4	13887.20	8.70	24.47
C.-g._sandstone_M2	14055.79	4148.72	3752.88	4	13906.10	15.60	25.02
C.-g._sandstone_M3	14035.88	4092.27	3777.45	4	13918.50	14.40	25.03
Dolostone_M1	6266.94	2365.42	2295.29	5	6227.70	24.20	15.01
Dolostone_M2	6251.14	2363.55	2295.32	5	6307.60	20.20	15.20
Dolostone_M3	6350.85	2354.40	2255.37	5	6712.10	4.30	16.02

https://doi.org/10.5194/egusphere-2026-3450
Preprint. Discussion started: 7 August 2026

	3D Micro-scan			Envelope density analysis			
Measurement ID	**Envelope volume**	**Surface area**	**Surface area incl. holes**	**Sample chamber (cf. Appendix B)**	**Envelope volume**	**Standard deviation**	**Ratio sample-to-Dry Flo**
	[mm³]	**[mm²]**	**[mm²]**		**[mm³]**	**[mm³]**	**[%]**
Clayey_marlstone_M1	2917.64	1345.45	1344.22	3	2892.00	9.40	21.09
Clayey_marlstone_M2	2917.27	1345.62	1344.95	3	2942.40	9.50	21.39
Clayey_marlstone_M3	2916.90	1345.37	1343.69	3	2973.30	5.40	21.61
Serpentinite_M1	9496.28	3092.02	2881.87	4	9419.70	15.20	19.59
Serpentinite_M2	9497.81	3092.53	2697.94	4	9379.10	18.80	19.55
Serpentinite_M3	9492.18	3098.29	2703.70	4	9321.80	17.10	19.46
Isotropic_claystone_M1	1123.13	733.89	733.69	2	1101.80	1.50	17.48
Isotropic_claystone_M2	1125.15	734.16	733.86	2	1096.30	1.10	17.45
Isotropic_claystone_M3	1127.00	734.94	734.94	2	1099.60	2.50	17.49
Sawn_tonalite_M1	8390.76	2756.53	2725.69	4	8111.60	12.10	17.88
Sawn_tonalite_M2	8376.04	2756.26	2678.22	4	8083.10	5.50	17.84
Sawn_tonalite_M3	8359.79	2861.75	2734.21	4	8114.90	14.50	17.94
Tonalite_M1	2898.93	1316.31	1038.75	4	2773.60	5.50	7.83
Tonalite_M2	2898.64	1312.85	958.56	4	2762.40	7.20	7.79
Tonalite_M3	2892.78	1320.26	922.11	4	2811.70	4.20	7.95
Phyllite_M1	9665.37	3730.64	3723.16	5	9525.40	4.30	10.19
Phyllite_M2	9658.36	3742.90	3525.86	5	9548.50	14.10	10.23
Phyllite_M3	9654.77	3745.04	3501.21	5	9449.90	7.70	10.11

https://doi.org/10.5194/egusphere-2026-3450
Preprint. Discussion started: 7 August 2026

Author contribution

LMA: conceptualization, formal analysis, investigation, writing (original draft preparation). ES: investigation, writing (review and editing). FD: supervision, writing (review and editing). HS: resources, writing (review and editing). MCD: supervision, conceptualization, writing (review and editing).

Competing interests

The authors declare that they have no conflict of interest.

Acknowledgements

We used ChatGPT (OpenAI), Google Gemini (Google), and Microsoft 365 Copilot (Microsoft) for grammatical and stylistic revision and for assistance in literature research. All sources were verified and evaluated by the authors.

References

Agin, G. J.: Representation and Description of Curved Objects, Dissertation, Computer Science Department, Stanford University, Stanford, USA, 140 pp., 1972.

Agin, G. J. and Highnam, P. T.: Movable Light-Stripe Sensor For Obtaining Three-Dimensional Coordinate Measurements, in: Robotics and Industrial Inspection, San Diego, United States, 23 May 1983, 326–333, 1983.

Allen, P. A. and Allen, J. R.: Basin Analysis: Principles and Application to Petroleum Play Assessment, 3rd Edition, 2nd ed., Blackwell Publishing Ltd, 549 pp., 2013.

Anton Paar GmbH: Envelope Density and Porosity of Solids Measured with Powder Flow Cell, 3 pp.

Artec 3D: Artec Micro, Datasheet, 5 pp., 2020.

Artec 3D: Artec Micro Manual: Web Manual, https://docs.artec-group.com/mic/, last access: 13 May 2025, 2019.

ASTM International: Standard Test Methods for Laboratory Standard Test Methods for Laboratory De termination of Density (Unit Weight) of Soil Specimens, West Conshohocken, PA, USA, 7 pp., https://doi.org/10.1520/D7263-09R18E02, 2016.

Bjørlykke, K. (Ed.): Petroleum Geoscience: From Sedimentary Environments to Rock Physics, 2nd ed., Springer, Berlin, Heidelberg, 662 pp., 2015.

Brown, E. T. (Ed.): ISRM: Suggested Methods: Rock characterization testing and monitoring, Pergamon Press, Oxford, UK, 211 pp., 1981.

Chen, C. H. and Kak, A. C.: Modeling and calibration of a structured light scanner for 3-D robot vision, in: Proceedings. 1987 IEEE International Conference on Robotics and Automation, Raleigh, NC, USA, 31 March 1987 - 03 April 1987, 807–815, 1987.

https://doi.org/10.5194/egusphere-2026-3450
Preprint. Discussion started: 7 August 2026

Deutsches Institut für Normung: Geometrische Produktspezifikationen (GPS) – Geometrische Produktspezifikationen (GPS) – Annahmeprüfung und Bestätigungsprüfung für Koordinatenmesssysteme (KMS): Teil 13 Optische 3D KMS, 17.040.30; 17.040.40, Beuth Verlag GmbH, Berlin, 74 pp., https://doi.org/10.31030/3274809, 2023.

Deutsches Institut für Normung: Geotechnische Erkundung und Untersuchung - Benennung und Beschreibung von Boden: Teil 1: Benennung und Beschreibung, 13.080.05; 93.020, 40 pp., https://doi.org/10.31030/3187022, 2020.

Deutsches Institut für Normung: Bewertung der Porengrößenverteilung und Porosität von Feststoffen mittels Quecksilberporosimetrie und Gasadsorption: Teil 1: Quecksilberporosimetrie, 19.120, Beuth Verlag GmbH, Berlin, 27 pp., https://doi.org/10.31030/3031674, 2019.

Deutsches Institut für Normung: Prüfverfahren für Naturstein – Bestimmung der Reindichte, der Rohdichte, der offenen Porosität und der Gesamtporosität, 73.020; 91.100.15, Beuth Verlag GmbH, Berlin, 12 pp., https://doi.org/10.31030/9831981, 2007.

Diara, F.: Structured-Light Scanning and Metrological Analysis for Archaeology: Quality Assessment of Artec 3D Solutions for Cuneiform Tablets, Heritage, 6016–6034, https://doi.org/10.3390/heritage6090317, 2023.

Dietmaier, A., Mattheis, J., Weller, D., Stober, I., Drews, M. C., and Baumann, T.: Visualization and semi-quantitative analysis of dissolution processes at artificial structures in carbonate rocks using optical, 3D micro-scanning and confocal laser scanning microscopy, Geotherm. Energy, https://doi.org/10.1186/s40517-025-00355-4, 2025.

Dunham, R. J.: Classification of Carbonate Rocks According to Depositional Texture, in: Classification of Carbonate Rocks—A Symposium, edited by: Ham, W. E., American Association of Petroleum Geologists, 108–121, https://doi.org/10.1306/M1357, 1962.

Eiríksson, E. R., Wilm, J., Pedersen, D. B., and Aanæs, H.: Precision and Accuracy Parameters in Structured Light 3-D Scanning, Int. Arch. Photogramm. Remote Sens. Spatial Inf. Sci., XL-5, 7–15, https://doi.org/10.5194/isprs-archives-XL-5-W8-7-2016, 2016.

Folk, R. L.: Practical Petrographic Classification of Limestones, AAPG Bulletin, 1–38, https://doi.org/10.1306/0BDA5C36-16BD-11D7-8645000102C1865D, 1959.

Georgopoulos, A., Ioannidis, C., and Valanis, A.: Assessing the performance of a structured light scanner, in: Proceedings of the ISPRS Commission V Mid-Term Symposium 'Close Range Image Measurement Techniques', Newcastle upon Tyne, UK, 21-24 June 2010, 250–255, 2010.

Gölder, D., Karakostis, F. A., and Falcucci, A.: Practical and technical aspects for the 3D scanning of lithic artefacts using micro-computed tomography techniques and laser light scanners for subsequent geometric morphometric analysis. Introducing the StyroStone protocol, PLoS ONE, https://doi.org/10.1371/journal.pone.0267163, 2022.

Grimm, W.-D. and Koch, R.: Bildatlas wichtiger Denkmalgesteine der Bundesrepublik Deutschland, 2nd ed., Arbeitshefte des Bayerischen Landesamtes für Denkmalpflege, 50, Lipp Verlag, München, Germany, 250 pp., 1990.

Homburg, T., Zwick, R., Mara, H., and Bruhn, K.-C.: Annotated 3D-Models of Cuneiform Tablets, Journal of Open Archaeology Data, 1–8, https://doi.org/10.5334/joad.92, 2022.

Jaeger, J. C., Cook, N., and Zimmermann, R. W.: Fundamentals of rock mechanics, 4th ed., Blackwell Publishing Ltd, 488 pp., 2007.

Limones, A., Çakmak, G., Fonseca, M., Roccuzzo, A., Cobo-Vázquez, C., Gómez-Polo, M., and Molinero-Mourelle, P.: Impact of scanning interruptions on accuracy of implant-supported full-arch scans: An in-vitro pilot study, JDR,

https://doi.org/10.5194/egusphere-2026-3450
Preprint. Discussion started: 7 August 2026

https://doi.org/10.1016/j.jdent.2024.105503, available at: https://www.sciencedirect.com/science/article/pii/S0300571224006730, 2025.

Mendricky, R. and Sobotka, J.: Accuracy Comparison of the Optical 3D Scanner and CT Scanner, Manufacturing Technology, 791–801, https://doi.org/10.21062/mft.2020.120, 2020.

Micromeritics Instrument Corporation: GeoPyc 1365: Envelope density analyzer, Operator manual, 96 pp., 2017.

Micromeritics Instrument Corporation: GeoPyc 1365: Envelope Density Analyzer, Brochure, Norcross, USA, 4 pp., 2016.

Micromeritics Instrument Corporation: GeoPyc 1360, München, Germany, V3, Part 136-42801-01, 1998.

Pettijohn, F. J., Potter, P. E., and Siever, R.: Petrography of Common Sands and Sandstones, in: Sand and Sandstone, edited by: Pettijohn, F. J., Potter, P. E., and Siever, R., Springer New York, New York, NY, 139–213, https://doi.org/10.1007/978-1-4612-1066-5_5, 1987.

Rocchini, C., Cignoni, P., Montani, C., Pingi, P., and Scopigno, R.: A low cost 3D scanner based on structured light, Computer Graphics Forum, 299–308, https://doi.org/10.1111/1467-8659.00522, 2001.

Sclatter, J. G. and Christie, P. A. F.: Continental Stretching: An explanation of the post-mid-cretaceous subsidence of the central north sea basin, JGR, 3711–3739, https://doi.org/10.1029/JB085iB07p03711, 1980.

Shamata, A. and Thompson, T.: Documentation and analysis of traumatic injuries in clinical forensic medicine involving structured light three-dimensional surface scanning versus photography, J. Forensic Leg. Med., 93–100, https://doi.org/10.1016/j.jflm.2018.05.004, available at: https://www.sciencedirect.com/science/article/pii/S1752928X18302737, 2018.

Shirai, Y.: Recognition of Polyhedrons with a Range Finder, Pattern Recognition, 243–256, https://doi.org/10.1016/0031-3203(72)90003-9, 1972.

Sivanandan, J. and Liscio, E.: Assessing Structured Light 3D Scanning using Artec Eva for Injury Documentation during Autopsy, ACSR, 5–13, 2016.

Sokovic, M. and Kopac, J.: RE (reverse engineering) as necessary phase by rapid product development, J. Mater. Process. Technol., 398–403, https://doi.org/10.1016/j.jmatprotec.2005.04.047, 2006.

Streckeisen, A.: Classification and nomenclature of plutonic rocks: Recommendations of the IUGS subcommission on the systematics of Igneous Rocks, Geol. Rundsch, 773–786, https://doi.org/10.1007/BF01820841, 1974.

Várady, T., Martin, Ralph, R, and Cox, J.: Reverse engineering of geometric models - an introduction, Computer-Aided Design, 255–268, https://doi.org/10.1016/S0010-4485(96)00054-1, 1997.

Verein Deutscher Ingenieure and Verband der Elektrotechnik Elektronik Informationstechnik: Optische 3D-Messsysteme Bildgebende Systeme mit punktförmiger Antastung, 17.040.30, Beuth Verlag GmbH, Berlin, 10 pp., 2002.

Weydt, L. M., Ramírez-Guzmán, Á. A., Pola, A., Lepillier, B., Kummerow, J., Mandrone, G., Comina, C., Deb, P., Norini, G., Gonzalez-Partida, E., Avellán, D. R., Macías, J. L., Bär, K., and Sass, I.: Petrophysical and mechanical rock property database of the Los Humeros and Acoculco geothermal fields (Mexico), Earth Syst. Sci. Data, 571–598, https://doi.org/10.5194/essd-13-571-2021, 2021.

Wiora, G.: Optische 3D-Messtechnik: Präzise Gestaltvermessung mit einem erweiterten Streifenprojektionsverfahren, Dissertation, Naturwissenschaftlich-Mathematische Gesamtfakultät, Ruprechts-Karls-Universität, Heidelberg, 126 pp., 2001.

https://doi.org/10.5194/egusphere-2026-3450
Preprint. Discussion started: 7 August 2026

Zoback, M. D.: Reservoir Geomechanics, Reservoir Geomechanics, Cambridge University Press, Cambridge, UK, 1-452, 2007.